MATERIALS SCIENCE

Phase behaviors of colloidal analogs of bent-core liquid crystals

Yang Yang,[1,2] Hanwen Pei,[3] Guangdong Chen,[1] Kyle Thomas Webb,[1] Luz J. Martinez-Miranda,[4] Isabel K. Lloyd,[4] Zhongyuan Lu,[3]* Kun Liu,[2]* Zhihong Nie[1]*

Bent-core liquid crystal (LC) molecules are known to form mesophases with fascinating polar order and supramolecular chirality despite the achiral nature of the mesogens. The assembly of colloidal particles with geometrical similarity to bent-core molecular mesogens not only provides new insights into the physical behaviors of atoms or molecules but also leads to new materials with broad applications. Despite tremendous progress in colloidal synthesis and assembly, there has been a lack of colloidal model systems of bent-core molecular mesogens for LC property discovery and application development. This article describes a systematic study on the phase behaviors of colloidal analogs of bent-core LC mesogens in both experiments and simulations. We demonstrated that bent rods with controlled bending angle (α) and aspect ratio (*L*/*D*, with *L* and *D* as the length and diameter of each rod arm, respectively) can spontaneously assemble into several typical banana phases including smectic A, smectic C, synclinic tilted antiferroelectric-like smectic, and twist smectic phases, resembling bent-core LC molecules. The formation and transition of these phases were found to be strongly dependent on the geometric parameters of rods. Phase diagrams were developed to illustrate the existence and stability range of all the LC phases in α and *L*/*D* space. This work opens the door to the development of novel complex types of molecular or colloidal self-organization and new functional materials with electro-optical or nonlinear optical properties.

INTRODUCTION

Colloidal particles can assemble into new functional materials with diverse applications such as photonics, phononics, sensing, and metamaterials (*1*). Moreover, colloidal particles are ideal model systems for exploring the organization and phase behavior of atoms and molecules (*2*–*4*). As an example, anisotropic colloids (for example, platelets, bowls, and rods) have been viewed as colloidal analogs of liquid crystal (LC) mesogens with different shapes (*5*–*7*). The assembly of these colloids produces a variety of conventional mesophases such as discotic, bowlic, nematic, columnar, and smectic phases, which are largely determined by their geometrical or topological constraints (for example, surface curvature or shape) (*8*–*10*). In particular, the phase behavior of rodlike colloids (for example, tobacco mosaic virus and inorganic rods) has been extensively studied both experimentally and computationally (*11*). It was found that colloidal rods can assemble into various nematic and smectic phases and that the transition between different phases is strongly dependent on the aspect ratio of the rods (*12*, *13*).

Bent-core (also called banana-shaped) LC molecules are known to form mesophases with fascinating polar order and supramolecular chirality despite the achiral nature of the mesogens (*14*, *15*). Typical mesophases that have been detected with bent-core molecules include such as biaxial nematic phases, ferroelectric/antiferroelectric (AF) smectic phases, chiral nematic or smectic phases, and twist grain boundary phases (*16*–*18*). Most of these phases have not been found in LC systems formed by conventional calamitic molecules. At much larger length scales, bent rods (BRs) with C_{2V} symmetry and an angular center closely resemble bent-core molecular mesogens in their geometrical form. The assembly of these BRs is expected to bring new properties that cannot be imagined in straight rods, particularly with regard to polarity and chirality. However, to date, the phase behaviors of BRs have not yet been assessed experimentally, largely because of current challenges in the large-scale fabrication of these rods (*19*).

This paper reports a systematic study on the phase behaviors of colloidal analogs of bent-core LCs using silica BRs with controlled geometry as a model system (*20*). We observed that the BRs assembled into various mesophases that are often seen in bent-core LC molecules (Fig. 1A). The equilibrium phases were found to be dictated by the geometrical features of BRs, namely bending angle (α) and aspect ratio (*L*/*D*, where *L* and *D* are the length and diameter of each rod arm, respectively; for straight rods, *L* is half of the total length). For straight rods (that is, α = 0°), a phase transition from smectic A (SmA) to smectic C (SmC) was observed when the *L*/*D* was increased. In contrast, the assembly of BRs produced three typical LC phases, in the sequence of SmA, synclinic tilted AF-like smectic (SmC_SP_A), and twist smectic (TSm) phases, with increasing α and *L*/*D*. As a representative example, the chirality formation in TSm phases from achiral building blocks (Fig. 1, B to D) is particularly striking and has been rarely reported in colloidal systems (*21*, *22*). The experimental results were supplemented by our Brownian dynamics simulations, and a good agreement was observed. Both experimental and computational results on the existence and stability range of all the phases were summarized in phase diagrams in α and *L*/*D* space. This work provides new insights into complex types of molecular and colloidal self-organization, as well as the fabrication of new functional materials with electro-optical or nonlinear optical properties (*14*).

[1]Department of Chemistry and Biochemistry, University of Maryland, College Park, MD 20742, USA. [2]State Key Laboratory of Supramolecular Structure and Materials, College of Chemistry, Jilin University, Changchun 130012, China. [3]State Key Laboratory of Supramolecular Structure and Materials, Institute of Theoretical Chemistry, Jilin University, Changchun 130021, China. [4]Department of Materials Science and Engineering, University of Maryland, College Park, MD 20742, USA.
*Corresponding author. Email: luzhy@jlu.edu.cn (Z.L.); kliu@jlu.edu.cn (K.L.); znie@umd.edu (Z.N.)

RESULTS

Banana LC phases assembled from BRs with various geometries

BRs with controlled α (0° to 48°) and *L*/*D* (2.5 to 10.2) were synthesized via a wet-chemical route we developed recently (see details in Materials and Methods) (*20*). Scanning electron microscopy (SEM) images (see

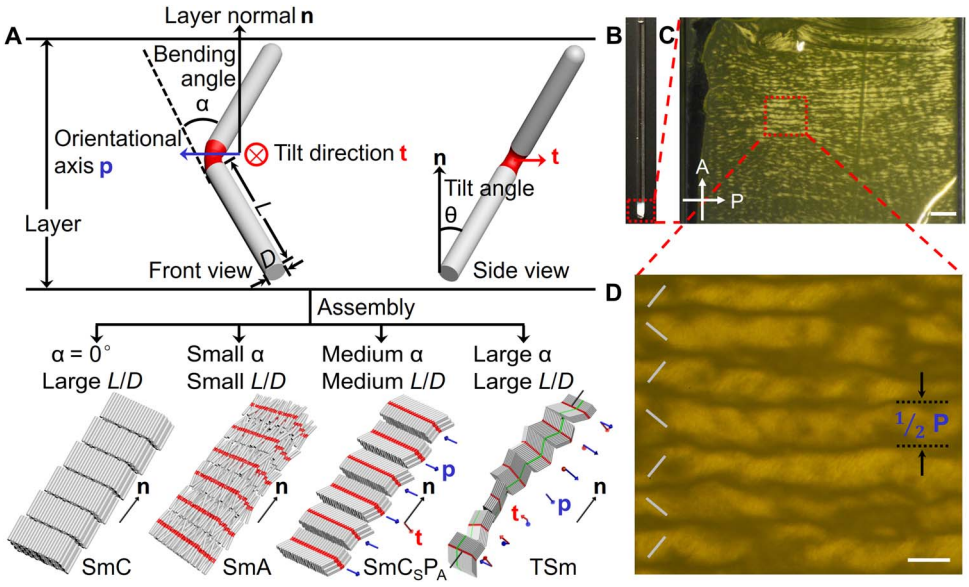

Fig. 1. Schematic illustration of the four typical LC phases assembled from BRs. (**A**) Schematic illustrations of the geometric and orientational parameters of BRs and the assembled SmC, SmA, SmC_SP_A, and TSm phases. The parameters, such as layer normal **n**, tilt direction **t**, and orientational axis **p**, define the chirality of the formed TSm phase. (**B**) Sediment of BRs dispersed in DMSO in a capillary tube. (**C** and **D**) Representative low (C) and high (D) magnification POM images of BRs with TSm phase in planar capillary. The spacing between two neighboring disclination lines [dotted lines in (D)] corresponds to $^1/_2$**P**. Scale bars, 200 μm (C) and 20 μm (D).

Fig. 2, A to D, and figs. S1 and S2) show some representative rods with different α and *L*/*D*. The BRs were dispersed in dimethyl sulfoxide (DMSO) in capillary tubes, and their assembly was triggered by slow sedimentation of BRs (Fig. 1B and fig. S3) (*6*, *12*). The characteristic LC phases started to form after ~20 days of sedimentation. After ~30 days of sedimentation, the volume fraction for the bottom ordered phase increased to ~50%, and this value largely remained constant when the system was kept standing for a prolonged time (fig. S4). The sediment phase exhibited fluidic nature of common LC materials, as reflected by the flowing phenomenon of rods inside upon tilting the capillary tube (fig. S5). The BRs can also be aligned to form LC phases by a shear, which is another LC characteristic property of BRs as conventional LC mesogens (fig. S6). Depending on α and *L*/*D*, the BRs assembled into a variety of LC mesophases, including SmC, SmA, SmC_SP_A, and TSm phases (Fig. 2, E to L). The long-range ordering of BRs was confirmed by polarized optical microscopy (POM). Upon a close inspection of the sediments, the striped regions in the colored domains, originating from the smectic layer structure of BRs, were observed in all these phases (Fig. 1, C and D, and fig. S7). In particular, the TSm phase with typical alternating zigzag band patterns can be distinguished from other smectic phases by the large-area POM images (*23*).

The detailed organizations of individual BRs within all the formed phases were characterized by localized POM (Fig. 2, E to H) and SEM (Fig. 2, I to L). The POM images in Fig. 1 (C and D) and fig. S7 were obtained by directly imaging the thick sediment phase (~0.2 mm in thickness) in the glass capillary. In this case, the focal plane was located at the top layers of the sample (that is, close to the inner wall of the capillary). To examine the detailed packing structures, small pieces of sediments, together with DMSO solvent trapped inside, were taken out from the capillary tube for a close inspection under POM (Fig. 2, E to H). Straight rods (α = 0°) assembled into the synclinic tilted SmC phase, in which rods are closely aligned side by side to form periodic layered structures (Fig. 2, A, E, and I). The localized POM (Fig. 2E) shows the striped texture and a relatively uniform birefringence color, which indicates the synclinic tilted packing of rods in the smectic layers. As directly shown in SEM image (Fig. 2I), the rods uniformly tilted to the layer normal, whereas the layer interface took up the synclinic configuration. BRs with small α (for example, α = 15°) organized into a uniaxial SmA phase with an average rod alignment perpendicular to the smectic layer (Fig. 2, B, F, and J). SmA phase also exhibits a striped texture and a uniform birefringence color that are similar to POM image of the SmC phase (Fig. 2F). The individual BRs, however, are tilted randomly within the smectic layer (as shown in Fig. 2J). The random tilting of BRs to the layer planes can be attributed to the relatively small energy barriers for the rotation of rods with less noticeable bending around their long axes within the layers. BRs with larger α (for example, α = 37°) exhibited the SmC_SP_A phase with biaxial packing of the rods (Fig. 2, C, G, and K). The formation of the biaxial smectic phase was confirmed by the characteristic texture, highly birefringent stripes with alternate colors running parallel to the layer planes in POM image (Fig. 2G). The different orientation of the two arms of BR is similar to the defects that are located in the boundaries of the two domains with opposite tilt directions of molecular mesogens, leading to the alternate colors between adjacent layers. The detailed packing of BRs is shown in Fig. 2K. BRs closely align in a side-by-side configuration and tightly pack along the orientational axis (**p**) with considerable positional and strong biaxial orientational ordering within each layer. The **p** of neighboring smectic layers is antiparallel, designated as AF-like without an overall steric moment. BRs tilt in the same direction in most adjacent layers, indicating that the phase is synclinic. The SmC_SP_A phase is thermodynamically stable because of the macroscopic nonpolar property with respect to the AF coupling, as well as the easy out-of-layer interlayer fluctuation of BRs with regard to the synclinic tilted structure.

When α is more significant (for example, α = 48°), it is remarkable that the BRs organized in the same chirality sense to form a TSm phase with locally defined handedness and helical pitches (**P**), although the constituent rods are achiral (Fig. 2, D, H, and L). Under POM, these structures exhibit the characteristic texture of the TSm phase: alternating

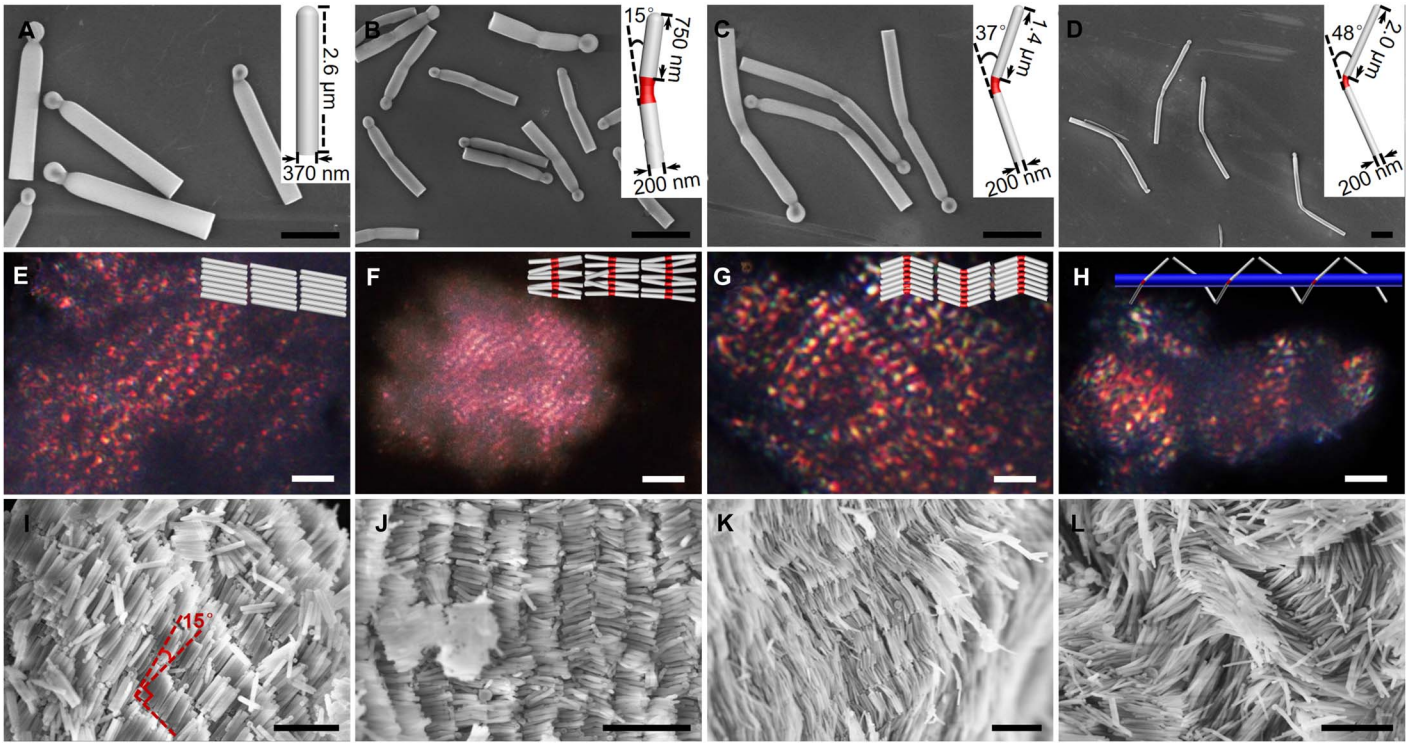

Fig. 2. BRs with different geometries and corresponding LC phases. (**A** to **D**) SEM images of representative rods with different α and *L*/*D*: (A) rod with α = 0° and *L*/*D* = 3.5, (B) BR with α = 15° and *L*/*D* = 3.8, (C) BR with α = 37° and *L*/*D* = 7.2, and (D) BR with α = 48° and *L*/*D* = 10.0. Insets in (A) to (D) are corresponding schematic illustrations of BRs. (**E** to **L**) POM images (E to H) and SEM images (I to L) of corresponding LC phases assembled from rods in (A) to (D): (E and I) SmC phase of rod in (A), (F and J) SmA phase of rod in (B), (G and K) SmC_SP_A phase of rod in (C), and (H and L) TSm phase of rod in (D). Insets in (E) to (H) are corresponding schematic illustrations of LC phases. Scale bars, 1 μm (A to D), 10 μm (E to H), and 4 μm (I to L).

zigzag band patterns at a low magnification (Fig. 1, C and D), as well as helical ribbon patterns, defined by the progression of a birefringent area followed by a dark area and subsequent birefringent area, at a high magnification (Fig. 2H). The average layer spacing of these zigzag patterns corresponds to half **P** ($^1/_2$**P**) of the TSm phase, which varies slightly from domain to domain (Fig. 1, C and D). For example, the helical structure in Fig. 2L shows a left-handedness and a **P** of ~22 μm. The chirality of the tilted phase is determined by the spatial relationship of the layer normal **n**, tilt direction **t**, and **p**, as illustrated in Fig. 1A. The formation of TSm phase was further confirmed by their optical activity in response to different polarization of light (fig. S8) and chiral signal in circular dichroism (CD) spectra of different locations of the mesophases (fig. S9).

Phase diagram and geometry effect based on experimental observations

The assembly phases of BRs were mapped out in a phase diagram in the space of α and *L*/*D* (Fig. 3A). Straight rods with *L*/*D* ≥ 3.5 preferentially organized into a conventional SmC phase, whereas straight rods with *L*/*D* < 3.5 assembled into the SmA phase (fig. S10), which is in good agreement with previously reported results about the phase behavior of straight rods (*12*, *13*). For BRs with small α and *L*/*D*, their assembly resembled straight rods to form the SmA phase because the rods can rotate freely along the long axis (fig. S11) (*24*). As α and/or *L*/*D* increased, the biaxial bent-core shape became more pronounced, and their rotational motion about the long axis of rods was largely constrained. This gave rise to the spontaneous orientation of rods along **p** within each smectic layer. This local orientational arrangement of the rods is characteristic of the SmC_SP_A phase (fig. S12). The tilt angle, θ, increased with the increase of α and/or *L*/*D*, which is consistent with previous experimental studies on bent-core LC molecules and computational simulations of bent colloidal rods (*14*, *24*, *25*). As shown in Fig. 3B, θ increased from 14° to 22° when α increased from 15° to 29° with a fixed *L*/*D* of 6.0. The θ value increased from 9° to 23° when *L*/*D* increased from 4.4 to 8.3 with a fixed α of 15°. The phase transition from the nonpolar SmA phase to the orientational SmC_SP_A phase of BRs, induced by the increase of α and/or *L*/*D*, is in good agreement with that of bent-core molecular mesogens (*18*, *24*, *26*). For the BRs with large α but small *L*/*D*, neither orientational nor positional order was found (fig. S13). The formation of the isotropic phase without ordering can be attributed to the reduced shape anisotropy of short rods.

With further increase of α (≥33°) and *L*/*D* (≥8.0), the achiral BRs, with a more pronounced bent-core shape, underwent spontaneous chiral symmetry breaking, resulting in the phase transition from the SmC_SP_A phase to the TSm phase (fig. S14). BRs are configurationally achiral, but they can adopt chiral organizations. Because of the two-dimensional geometry of BRs, two spontaneous symmetry-breaking transitions occur in the layers: orientational ordering and intralayer tilting of BRs. The **t** and **p** of BRs periodically vary by a distinct angle from layer to layer to break reflection symmetry, which gives rise to chiral layers with a locally defined handedness. BRs can tilt with respect to **n** in two equivalent ways that are mirror images of each other, thus leading to the formation of right- and left-handed chiral domains with equal probability (fig. S14). In each chiral domain, BRs with arrangements of uniform chirality sense can pack more efficiently than the other. It is worth noting that the presence of both enantiomeric local structures with equal probability led to the achiral feature of the macroscopic samples. This

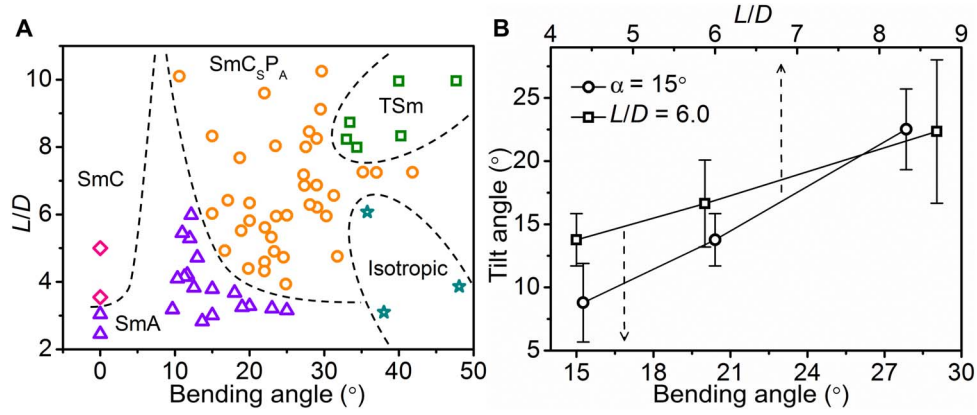

Fig. 3. Effect of BR geometry on experimental phase diagram. (**A**) Experimental phase diagram of symmetric BRs as a function of α and *L*/*D*. The dashed lines indicate superficial boundaries between phases. (**B**) Tilt angle θ as a function of α and *L*/*D* of BRs in the SmC_SP_A phase.

phenomenon is in agreement with the previous studies on bent-core LC molecules (*27*) and theoretical exploration of bent-core rods (*25*). The formation of the TSm phase enables the most efficient escape from macroscopic orientational order compared with a phase in a symmetric state (*17*, *25*). To the best of our knowledge, this presents the first demonstration of α-dependent twist LC phase formation of achiral bent core–shaped colloids. Overall, these results manifest the subtle effect of rod geometry on the phase behavior of BRs.

LC phase behavior of asymmetric BRs

For asymmetric BRs with arms of different lengths, only conventional SmA phases were observed. The asymmetric BRs packed in an interdigitated arrangement within the smectic layers (fig. S15). Moreover, the packing of asymmetric BRs became loose to accommodate BRs (fig. S16). As a result, the interlayer spacing was found to be much larger than the lengths of the BRs. Our systematic study of BRs with a range of α (15° to 45°) and *L*/*D* (2.6 to 10.1) indicates that the geometric parameters of asymmetric BRs have little effect on the phase behavior.

Computational simulations based on coarse-grained Brownian dynamics model

We simulated the assembly phases of BRs with different geometric parameters using a coarse-grained Brownian dynamics model (see details in Materials and Methods) (*28*). Briefly, the BRs are modeled as a series of beads bonded rigidly together into a BR geometry with various α and *L*/*D* in accordance to the size and shape of real BRs (fig. S17). The interactions between BRs are purely repulsive Weeks-Chandler-Andersen (WCA) potential. All simulations were carried out in a cubic cell with periodic boundary conditions. To simulate the phase condition with high density, the length of box size was slowly shrunk to a target dimension in a certain time step.

Figure 4 shows six characteristic snapshots of assembled BRs with different α and *L*/*D*. First, our simulation confirms the formation of all the phases observed in experiments. Second, our simulation indicates that the assembly phases of BRs are strongly dependent on α (Fig. 4, A to D). When *L*/*D* is fixed as 4, straight rods (α = 0°) accommodate in a tilted SmC phase (Fig. 4A). BRs with α = 10° form a SmA phase due to minimal constraints on the rotational motion of the BRs (Fig. 4B), whereas BRs with α = 25° experience strong rotational constraints, resulting in the formation of the biaxially ordered AF phase (Fig. 4C). BRs with α = 50° exhibit an isotropic phase with a disordered structure because the formation of the smectic phase causes a free energetic penalty due to the decrease in the rotational and translational entropy of these BRs (Fig. 4D). Third, it was found that variation in *L*/*D* can solely drive the transition of the assembly phases of BRs (see Fig. 4, D to F, and fig. S20). Take BRs with α = 50° as an example; short rods (*L*/*D* = 4) exhibit the isotropic phase (Fig. 4D). In contrast, rods with a medium length (*L*/*D* = 6) remain in the SmC_SP_A phase (Fig. 4E), whereas long rods (*L*/*D* = 10) form the TSm phase (Fig. 4F). The orientation parameter $\chi = \sum_{i=1}^{N}|\cos\beta_i|/N$, where *N* is the layer number and β is the orientational angle between neighboring layers, reflects the average orientational angle between neighboring layers (see detailed definition in note S2). It is calculated to describe the phase transition between the biaxially ordered AF phase and the TSm phase (see details in note S4). A χ value close to 1.0 suggests β approaching 180° or 0°, whereas the value of χ should be less than 1.0 when β is diverging from these two values. In Fig. 4G, the plateau value of χ around 0.95 indicates that the system does not have the chiral symmetry with small α, therefore it is assigned to the orientational smectic phase. However, when α increases to 30°, χ reduces to a lower plateau value of around 0.7, corresponding to the twist phase. The variation of χ indicates the transition from the biaxially ordered AF phase to the TSm phase.

Phase diagram and geometry effect based on computational simulations

The phase transitions in a range of α and *L*/*D* observed in simulations were summarized in a phase diagram (note S5 and Fig. 5). The phase regions are in good agreement with the experimental phase diagram. For the symmetric BRs, the phase behavior is determined by both α and *L*/*D*. The SmA phase is stable only when α and *L*/*D* are both small, which means that the BRs adopt a nearly straight rodlike shape. When the bent shape is prominent, the formation of the SmA phase is suppressed, and that of the two distinct banana phases (namely the SmC_SP_A phase and the TSm phase) is strongly promoted. The SmC_SP_A phase is formed when α and/or *L*/*D* are increased. As *L*/*D* is increased, the SmA-SmC_SP_A transitions shift to a low α. Vice versa, the SmA-SmC_SP_A transitions shift to a low *L*/*D* with the increase of α. The TSm phase is formed with further increasing α and *L*/*D*. It is worth mentioning that the individual BRs are achiral, and the chirality of the structure arises from the arrangement of the BRs within the smectic layers. Overall, the theoretical modeling reproduces our experimental observations and offers realistic descriptions of the five typical phases formed by BRs and the transitions between these phases.

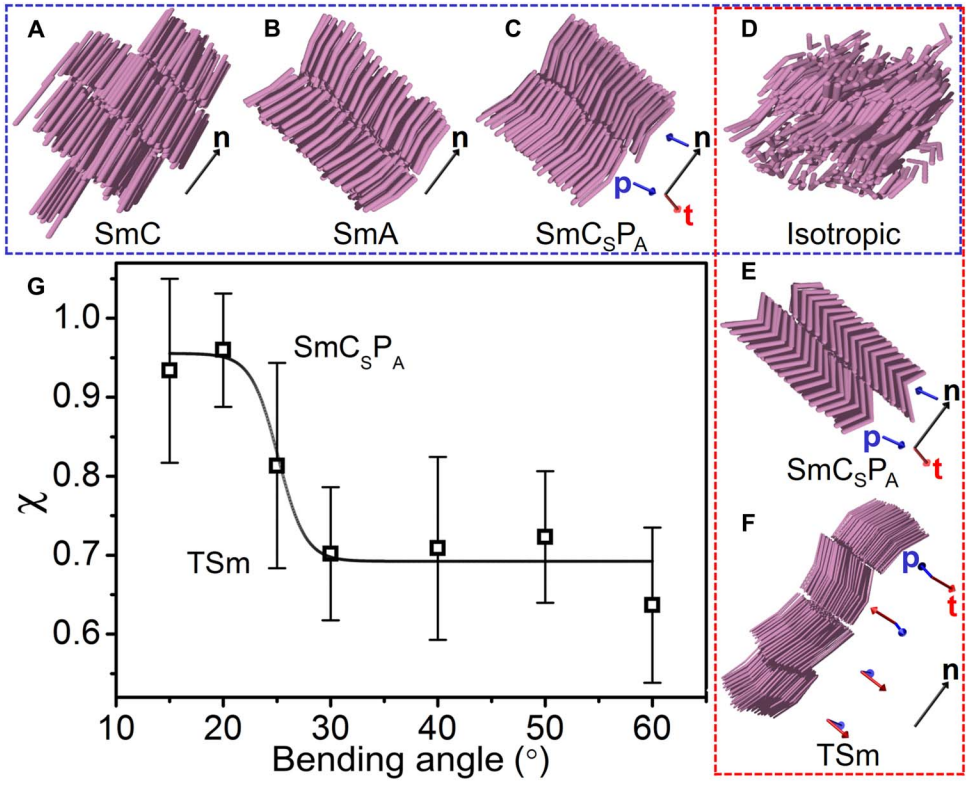

Fig. 4. LC phases observed in Brownian dynamics simulations. Simulation results of LC phases assembled from rods (**A** to **D**) with $L/D = 4$ but different α: (A) rod with α = 0° in SmC phase, (B) rod with α = 10° in SmA phase, (C) rod with α = 25° in SmC_SP_A phase, and (D) rod with α = 50° in isotropic phase; rods (**E** and **F**) with the same α as rod in (D): (E) rod with $L/D = 6$ in SmC_SP_A phase and (F) rod with $L/D = 10$ in TSm phase. (**G**) The orientation parameter χ varies with α of the BRs with $L/D = 8$.

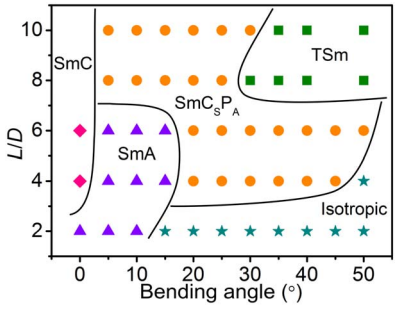

Fig. 5. Phase diagram given by simulations. Simulation phase diagram of symmetric BRs as a function of α and L/D. The solid lines are drawn to guide the eye on boundaries between phases.

DISCUSSION

In summary, we have systematically examined the phase behaviors of colloidal analogs of bent-core LC molecules and determined the role of rod geometry in the formation of different ordering phases. Our experimental results showed that BRs with α ranging from 0° to 48° behave like bent-core mesogens to assemble into a variety of classic LC phases including the SmC, SmA, SmC_SP_A, and TSm phases. The phases and onset of phase transitions were found to be strongly dependent on the geometric parameters (that is, α and L/D) of the rods. Notably, Brownian dynamics simulation was in agreement with experimental observations, thus allowing for the prediction of BR phase formation. This work suggests that BRs can serve as a model of molecular systems for understanding the physical properties such as phase transition and assembly behaviors of molecules. On the other hand, inspirations can be taken from molecular system for the design of complex colloidal structures or phases through the entropy-driven assembly of BRs (*8*–*10*). For instance, mixture of molecular mesogens with distinct shapes exhibits LC phases and phase transitions that may not be observed in the system containing only one of the constituent components (*29*, *30*). This suggests the promise of achieving complex assembly using mixed colloidal building blocks (for example, straight rods and BRs) in future research.

From the technological standpoints, the assembly of bent-core particles offers great opportunities for the development of structured composite materials with pre-engineered optical and mechanical properties (*14*). For instance, dispersions of colloidal particles in the molecular LC host medium represent an emerging class of functional soft matter. When bent-core particles are used, novel elastic colloidal interactions could be induced to promote the formation of ordered architectures (for example, low-symmetry colloidal crystals) of colloidal assemblies due to the orientational elasticity of LC molecules (*31*, *32*). Because colloidal particles are more susceptible to external fields (for example, electric field) than molecules, the resulting composite materials could find applications in such as tunable photonic crystals, flexible information displays, light shutters, metamaterials, and other switchable devices (*1*, *3*, *11*).

MATERIALS AND METHODS

Synthesis of BRs

BRs were synthesized using an emulsion-templated wet-chemical approach through temperature modulation we recently developed (*20*). In a typical experiment, 500 mg of polyvinylpyrrolidone (M_n = 40,000 g/mol;

Sigma-Aldrich) was dissolved in 5.0 ml of 1-pentanol (99%; Sigma-Aldrich) in a 10-ml glass vial under sonication. A total of 140 μl of deionized water (18.2 megohms), 50 μl of 0.18 M sodium citrate dihydrate aqueous solution (99%; Sigma-Aldrich), 475 μl of anhydrous ethanol (Pharmco-Aaper), and 60 μl of ammonium hydroxide solution (28 weight %; Sigma-Aldrich) were added to the glass vial and mixed (vortex stirrer) for 1 min. After the mixture was left standing for 5 min to release the gas bubbles, 50 μl of tetraethyl orthosilicate (98%; Sigma-Aldrich) was added, and the solution was then gently shaken for 30 s. The L of each arm varied from 500 nm to 2.5 μm of BRs can be individually controlled by tuning the reaction time. The D of BRs can be tuned from 150 to 370 nm by increasing the amount of ammonium hydroxide. The α of BRs in a range of 0° to 48° can be adjusted by varying the strength of perturbation in the reaction temperature (25° to 70°C) during the rod growth. The higher the temperature during perturbation period of time produces the larger α. As an example, for BRs with α = 45° and L/D = 7.0, the reaction mixture was incubated at 25°C for 2 hours, 65°C for 5 min, and 20°C for another 4 hours.

Purification

The as-synthesized BRs were then purified by centrifugation at 6000 rpm for 10 min. The precipitated rods were then washed three times with ethanol at 3000 rpm. Finally, the rods were centrifuged at 1000 rpm for 10 min to remove small particles and other lightweight impurities.

Assembly of BRs and straight rods into LCs

The BR or straight rod dispersions in DMSO (99.9%; Fisher Chemical) with a volume fraction of 30% were loaded into one end–sealed glass capillaries (Stuart) of 1.9 mm in outside diameter, 1.3 mm in inside diameter, and 100 mm in length and rectangular capillaries (VitroCom) of 2.0 mm in width, 0.2 mm in inner thickness, 0.14 mm in wall thickness, and 50 mm in length. After filling, the other ends of capillaries were closed by melting. Then, the capillaries were left in a vertical position for sedimentation of BRs. After 1 month, the capillaries were opened, and the sediment was taken out for POM characterization and slowly dried in air at room temperature for SEM characterizations. The samples in rectangular capillaries were directly used for POM characterization.

Characterizations

BRs and their assemblies were imaged by using a Hitachi SU-70 Schottky field emission gun SEM at an operation voltage of 10 kV. POM images were obtained by using an Olympus BX50F4 Microscope with a polarizer. CD spectra were recorded using a Jasco J-810 CD spectrometer. A scan speed of 500 nm/min was used.

Computer simulations

In Brownian dynamics simulations, each arm of the BRs was built by freezing linearly arranged spherical beads of diameter σ. The neighboring beads were separated by a distance of 0.97σ. A "core" bead is located at the center of a BR (fig. S17). The length of each arm was set to be the same (that is, $L_1 = L_2$). α is the bending angle of the BR. Each BR was treated as a rigid body in simulations. Nonbonded interactions between BR beads were described by WCA potential (*33*, *34*). The WCA potential is the 12-6 Lennard-Jones potential truncated at the energy minimum and shifted vertically by ε/k_BT (Boltzmann constant × temperature); it is a purely repulsive potential featuring the volume occupied by the BRs. The Brownian dynamics of a rigid body in the canonical ensemble was adopted to conduct the simulations. The implicit solvent model was adopted. The details of the simulation method can be referred to the study of Zhang *et al.* (*28*). The length and energy units of the simulation system are σ and ε, respectively. The time step is in units of $\sigma\sqrt{m/\varepsilon}$, whereas the unit of temperature is ε/k_B. The leapfrog algorithm of a rigid body with a time step of $\Delta t = 0.01$ was adopted to integrate the equations of motion. Bent-core rods in the initial configuration of the simulation were randomly generated in the simulation box. The system was then equilibrated at a higher temperature until it was fully disordered. After that, the temperature was decreased from $1.05k_B/\varepsilon$ to $0.5k_B/\varepsilon$, with an interval of $\Delta T = 0.05k_B/\varepsilon$ every 3×10^6 time steps. Then, we repeatedly increased and decreased the temperature between $0.5k_B/\varepsilon$ and $0.85k_B/\varepsilon$ every 2×10^6 time steps (six cycles in each simulation) to anneal the system. Then, the system was further equilibrated for 1×10^7 time steps. The number density of the initial configuration (≈0.2) is much lower than the target density. We then isotropically shrank the simulation box until the system reached the target density (≈0.7 particles/σ^3) in 1×10^8 time steps. The volume fraction (F) can be converted to the number density (ρ) of particles (particles per unit volume) by the equation of $F = \rho V_{all}/N_{beads}$, where V_{all} is the particle volume ($V_{all} = 2L\pi r^2 + 4\pi r^3/3$, L is the arm length of rod, and r is the radius of spherical beads that construct the particle), and N_{beads} is the number of spherical beads that construct the particle. The experimental volume fraction of ~50% corresponded to a number density of ~0.7 particles/σ^3. We therefore chose a target number density of 0.7 particles/σ^3 of the sediment phase in simulation. For bent-core rods with long arm lengths (≥8σ) or large α (≥20°), the system may be easily trapped in a metastable state. To solve this problem, we started the simulation from the initial configuration with a higher density (0.5 in our simulation). In this scheme, bent-core rods in the initial configuration were generated parallel to the z axis, and the bent-core rods in each layer were placed in the same orientation. In this manner, some metastable states were directly avoided from the very beginning of the simulation. Box lengths were set as the same in both x and y directions. To identify the proper orientation of interlayers, we selected the configuration whose pressure components are similar in x, y, and z directions. For example, in the system with α = 60° and arm length of 8σ as an example, we conducted a series of simulations varying with different box lengths in the z direction (L_z) under the same simulation conditions. In the simulation, pressure components in the x, y, and z directions were calculated, as shown in table S1. The pressure components were similar in all directions when L_z equals to 90σ and 91σ. The tensor order parameter Q (note S1) was calculated to characterize the LC phases of bent-core rods with uniaxial or biaxial order (see details in note S3 and figs. S18 and S19). The orientation parameter, χ, was calculated to distinguish the twist phase and the non-TSm one (notes S2 and S4 and Fig. 4G).

SUPPLEMENTARY MATERIALS

Supplementary material for this article is available at http://advances.sciencemag.org/cgi/content/full/4/5/eaas8829/DC1

fig. S1. SEM images of representative BRs with different geometries.
fig. S2. SEM images of representative asymmetric BRs with different geometries.
fig. S3. Sedimentation of BRs.
fig. S4. Volume fraction of BRs in the bottom ordered phase.
fig. S5. Flow feature of the LC phase.
fig. S6. Shear-induced LC formation.
fig. S7. POM images showing the long-range ordering of BRs in the SmC_SP_A phase.
fig. S8. Optical activity of the TSm phase.
fig. S9. CD spectra of the TSm phase.

REFERENCES AND NOTES

1. M. A. Boles, M. Engel, D. V. Talapin, Self-assembly of colloidal nanocrystals: From intricate structures to functional materials. *Chem. Rev.* **116**, 11220–11289 (2016).
2. V. N. Manoharan, M. T. Elsesser, D. J. Pine, Dense packing and symmetry in small clusters of microspheres. *Science* **301**, 483–487 (2003).
3. F. Li, D. P. Josephson, A. Stein, Colloidal assembly: The road from particles to colloidal molecules and crystals. *Angew. Chem. Int. Ed.* **50**, 360–388 (2011).
4. Q. Chen, J. K. Whitmer, S. Jiang, S. C. Bae, E. Luijten, S. Granick, Supracolloidal reaction kinetics of Janus spheres. *Science* **331**, 199–202 (2011).
5. F. M. van der Kooij, K. Kassapidou, H. N. W. Lekkerkerker, Liquid crystal phase transitions in suspensions of polydisperse plate-like particles. *Nature* **406**, 868–871 (2000).
6. M. Marechal, R. J. Kortschot, A. F. Demirörs, A. Imhof, M. Dijkstra, Phase behavior and structure of a new colloidal model system of bowl-shaped particles. *Nano Lett.* **10**, 1907–1911 (2010).
7. K. E. Shopsowitz, H. Qi, W. Y. Hamad, M. J. MacLachlan, Free-standing mesoporous silica films with tunable chiral nematic structures. *Nature* **468**, 422–425 (2010).
8. P. F. Damasceno, M. Engel, S. C. Glotzer, Predictive self-assembly of polyhedra into complex structures. *Science* **337**, 453–457 (2012).
9. J. Henzie, M. Grünwald, A. Widmer-Cooper, P. L. Geissler, P. Yang, Self-assembly of uniform polyhedral silver nanocrystals into densest packings and exotic superlattices. *Nat. Mater.* **11**, 131–137 (2012).
10. V. N. Manoharan, Colloidal matter: Packing, geometry, and entropy. *Science* **349**, 1253751 (2015).
11. H. N. W. Lekkerkerker, G. J. Vroege, Liquid crystal phase transitions in suspensions of mineral colloids: New life from old roots. *Philos. Trans. A Math. Phys. Eng. Sci.* **371**, 20120263 (2013).
12. A. Kuijk, A. van Blaaderen, A. Imhof, Synthesis of monodisperse, rodlike silica colloids with tunable aspect ratio. *J. Am. Chem. Soc.* **133**, 2346–2349 (2011).
13. A. Kuijk, D. V. Byelov, A. V. Petukhov, A. van Blaaderen, A. Imhof, Phase behavior of colloidal silica rods. *Faraday Discuss.* **159**, 181–199 (2012).
14. R. A. Reddy, C. Tschierske, Bent-core liquid crystals: Polar order, superstructural chirality and spontaneous desymmetrisation in soft matter systems. *J. Mater. Chem.* **16**, 907–961 (2006).
15. J. W. Goodby, P. J. Collings, T. Kato, C. Tschierske, H. F. Gleeson, P. Raynes, *Handbook of Liquid Crystals* (Wiley-VCH, ed. 2, 2014).
16. P. I. C. Teixeira, A. J. Masters, B. M. Mulder, Biaxial nematic order in the hard-boomerang fluid. *Mol. Cryst. Liq. Cryst. Sci. Technol. Sect. A* **323**, 167–189 (1998).
17. C. Greco, A. Ferrarini, Entropy-driven chiral order in a system of achiral bent particles. *Phys. Rev. Lett.* **115**, 147801 (2015).
18. Y. Lansac, P. K. Maiti, N. A. Clark, M. A. Glaser, Phase behavior of bent-core molecules. *Phys. Rev. E* **67**, 011703 (2003).
19. A. Chakrabarty, A. Konya, F. Wang, J. V. Selinger, K. Sun, Q.-H. Wei, Brownian motion of boomerang colloidal particles. *Phys. Rev. Lett.* **111**, 160603 (2013).
20. Y. Yang, G. Chen, L. J. Martinez-Miranda, H. Yu, K. Liu, Z. Nie, Synthesis and liquid-crystal behavior of bent colloidal silica rods. *J. Am. Chem. Soc.* **138**, 68–71 (2016).
21. Z. Xu, C. Gao, Graphene chiral liquid crystals and macroscopic assembled fibres. *Nat. Commun.* **2**, 571 (2011).
22. N. Donkai, H. Hoshino, K. Kajiwara, T. Miyamoto, Lyotropic mesophase of imogolite, 3 observation of liquid crystal structure by scanning electron and noval polarized optical microscopy. *Makromol. Chem.* **194**, 559–580 (1993).
23. S.-W. Lee, B. M. Wood, A. M. Belcher, Chiral smectic C structures of virus-based films. *Langmuir* **19**, 1592–1598 (2003).
24. S. J. Johnston, R. J. Low, M. P. Neal, Computer simulation of polar bent-core molecules. *Phys. Rev. E* **66**, 061702 (2002).
25. A. V. Emelyanenko, M. A. Osipov, Origin of spontaneous polarization, tilt, and chiral structure of smectic liquid-crystal phases composed of bent-core molecules: A molecular model. *Phys. Rev. E* **70**, 021704 (2004).
26. A. Eremin, H. Nádasi, G. Pelzl, S. Diele, H. Kresse, W. Weissflog, S. Grande, Paraelectric–antiferroelectric transitions in the bent-core liquid-crystalline materials. *Phys. Chem. Chem. Phys.* **6**, 1290–1298 (2004).
27. D. R. Link, G. Natale, R. Shao, J. E. Maclennan, N. A. Clark, E. Körblova, D. M. Walba, Spontaneous formation of macroscopic chiral domains in a fluid smectic phase of achiral molecules. *Science* **278**, 1924–1927 (1997).
28. Z. Zhang, M. A. Horsch, M. H. Lamm, S. C. Glotzer, Tethered nano building blocks: Toward a conceptual framework for nanoparticle self-assembly. *Nano Lett.* **3**, 1341–1346 (2003).
29. R. Pratibha, N. V. Madhusudana, B. K. Sadashiva, An orientational transition of bent-core molecules in an anisotropic matrix. *Science* **288**, 2184–2187 (2000).
30. P. K. Maiti, Y. Lansac, M. A. Glaser, N. A. Clark, Induced anticlinic ordering and nanophase segregation of bow-shaped molecules in a smectic solvent. *Phys. Rev. Lett.* **88**, 065504 (2002).
31. C. P. Lapointe, T. G. Mason, I. I. Smalyukh, Shape-controlled colloidal interactions in nematic liquid crystals. *Science* **326**, 1083–1086 (2009).
32. H. Mundoor, B. Senyuk, I. I. Smalyukh, Triclinic nematic colloidal crystals from competing elastic and electrostatic interactions. *Science* **352**, 69–73 (2016).
33. J. Xu, R. L. B. Selinger, J. V. Selinger, R. Shashidhar, Monte Carlo simulation of liquid-crystal alignment and chiral symmetry-breaking. *J. Chem. Phys.* **115**, 4333–4338 (2001).
34. J. D. Weeks, D. Chandler, H. C. Andersen, Role of repulsive forces in determining the equilibrium structure of simple liquids. *J. Chem. Phys.* **54**, 5237–5247 (1971).
35. P. J. Camp, M. P. Allen, A. J. Masters, Theory and computer simulation of bent-core molecules. *J. Chem. Phys.* **111**, 9871–9881 (1999).
36. M. P. Allen, Computer simulation of a biaxial liquid crystal. *Liq. Cryst.* **8**, 499–511 (1990).
37. Y. Takanishi, A. Ikeda, H. Takezoe, A. Fukuda, Higher smectic-layer order parameters in liquid crystals determined by x-ray diffraction and the effect of antiferroelectricity. *Phys. Rev. E* **51**, 400–406 (1995).

Acknowledgments: We acknowledge the support from the Maryland NanoCenter and its AIMLab. **Funding:** Z.N. and I.K.L. acknowledges financial support of grant R21DE024632A from National Institute for Dental and Craniofacial Research. Z.N. and K.L. acknowledge financial support from Open Project of State Key Laboratory for Supramolecular Structure and Materials (SKLSSM 201618). K.L. thanks the National Natural Science Foundation of China (21474040 and 21674042) and China's Thousand Talent Plan for financial support. K.L. and Z.L. acknowledge financial support from the National Natural Science Foundation of China (21534004). **Author contributions:** Y.Y., Z.L., K.L., and Z.N. designed the research. Y.Y., H.P., and G.C. performed the research. Y.Y., H.P., G.C., K.T.W., L.J.M.-M., I.K.L., Z.L., K.L., and Z.N. analyzed the data. Y.Y., Z.L., K.L., and Z.N. wrote the paper. **Competing interests:** The authors declare that they have no competing interests. **Data and materials availability:** All data needed to evaluate the conclusions in the paper are present in the paper and/or the Supplementary Materials. Additional data related to this paper may be requested from the authors.

Submitted 30 December 2017
Accepted 20 March 2018
Published 11 May 2018
10.1126/sciadv.aas8829

Citation: Y. Yang, H. Pei, G. Chen, K. T. Webb, L. J. Martinez-Miranda, I. K. Lloyd, Z. Lu, K. Liu, Z. Nie, Phase behaviors of colloidal analogs of bent-core liquid crystals. *Sci. Adv.* **4**, eaas8829 (2018).

Science Advances

Phase behaviors of colloidal analogs of bent-core liquid crystals

Yang Yang, Hanwen Pei, Guangdong Chen, Kyle Thomas Webb, Luz J. Martinez-Miranda, Isabel K. Lloyd, Zhongyuan Lu, Kun Liu and Zhihong Nie

Sci Adv **4** (5), eaas8829.
DOI: 10.1126/sciadv.aas8829